JOURNAL OF MATERIALS SCIENCE 27 (1992) 5681–5691

Mechanical and tribological properties of zinc–aluminium metal-matrix composites

S. H. J. LO, S. DIONNE, M. SAHOO
CANMET/MTL, Energy, Mines and Resources, 568 Booth Street, Ottawa, Ontario, Canada K1A 0G1

H. M. HAWTHORNE
Tribology and Mechanics Laboratory, National Research Council, 3650 Wesbrook Mall, Vancouver, British Columbia, Canada V6S 2L2

Recently, commercial Zn–Al foundry alloys such as ZA-27 have found increasing use for many applications and have competed effectively against copper, aluminium and iron-based foundry alloys. However, the elevated temperature (> 100 °C) properties of zinc–aluminium alloys are unsatisfactory and restrict their use in some applications. One viable approach to improving the elevated temperature properties is to reinforce the zinc–aluminium alloys with alumina fibres. In this investigation, the mechanical properties of a Zn–Al alloy reinforced with alumina fibres were evaluated. Tensile, compression and impact properties were determined at 25, 100 and 150 °C. Lubricated wear tests were also performed on the unreinforced alloy and composites. It was found that although fibre reinforcement did result in some improvement of tensile and compression properties at elevated temperatures, the composites had poor toughness and ductility. The presence of a brittle SiO_2 layer at the fibre/matrix interfaces resulted in fibre/matrix decohesion under tensile loading, impairing the performance of the reinforced materials. Some improvement in wear resistance was noted for the composite materials but fibre reinforcement did not yield significant improvement in fatigue resistance.

1. Introduction

Zinc–aluminium (Zn–Al) based alloys have found considerable industrial use. This is primarily due to their excellent fluidity, castability, and good mechanical properties [1]. Initially, Zn–Al alloys such as ZA-35 were developed for their wear resistance and bearing properties. Later, Zn–Al alloys with various contents of aluminium, such as ZA-8, ZA-12 and ZA-27, were developed for casting prototype parts. The ZA-27 alloy is known for its high strength/density ratio and can, therefore, compete satisfactorily with other foundry alloys such as copper, aluminium or cast iron.

Despite the attractive room-temperature properties of Zn–Al alloys, the elevated temperature mechanical properties were found to be unsatisfactory. Essentially, degradation of tensile strength and creep resistance occurs at temperatures around 100 °C. Considering their low melting temperature, a temperature of 100 °C corresponds to about 0.49 T_m for some of the alloys. With this limitation, the extent of application of the alloys is restricted to those for ambient service temperature environments.

An attractive possibility of improving the high-temperature properties of Zn–Al alloys up to 150 °C is by fibre reinforcement to form composite materials. The potential advantages which can be gained include improvement in strength, modulus of elasticity, creep and wear resistance [2–4]. In the present work, a Zn–Al based alloy with approximately 32 wt % aluminium was studied and metal-matrix composites (MMCs) were produced by squeeze-casting with alumina fibres.

2. Experimental procedure

All of the materials evaluated in this work were fabricated by JPL Transportation Products Inc., Engine Products Group, Cleveland, OH, for Noranda Technology Centre. The chemical composition (wt %) of the Zn–Al alloy is given in Table I.

Squeeze-cast samples were in the form of discs, with dimensions of 130 mm diameter and 40 mm thick. In addition to the Zn–32Al discs, discs reinforced with alumina fibres were also fabricated by squeeze-casting. Details of the squeeze-casting process were not made available. The reinforced discs were produced using 12 and 24 vol % alumina fibre preforms made by ICI. The Saffil alumina fibres in the preforms, were reported to consist of 96%–97% delta alumina and 3% –4% silica (ICI product literature) which was confirmed by microprobe analysis. Closer examination of fibre surfaces revealed the presence of patches and films of SiO_2 (Fig. 1), which is used as the binder material for bonding the fibres to form a three-dimensional network of inter-connecting fibres.

0022–2461

TABLE I

Al	Cu	Fe	Mg	Si	Zn
32.5	2.06	0.065	0.012	0.012	balance

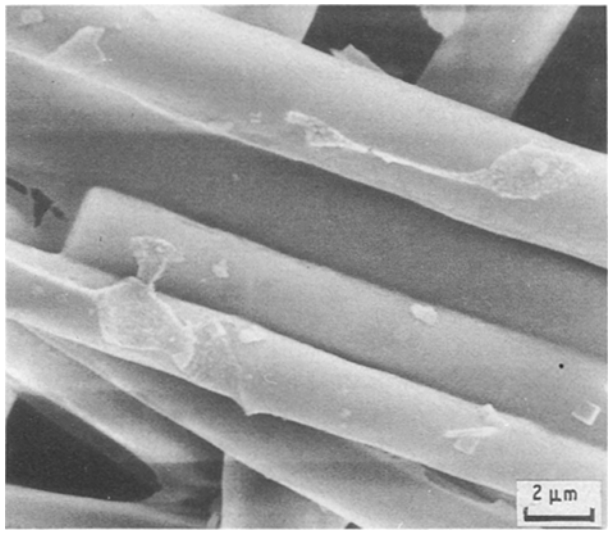

Figure 1 Scanning electron micrographs of Al_2O_3 fibre preform showing patches and films of SiO_2.

For tensile testing, sub-size specimens proportional to ASTM standard E-8, with 6.35 mm gauge diameter, 25.4 mm gauge length and threaded ends were machined from the squeeze-cast discs. Testing was performed on an MTS model 810 tensile testing machine at a strain rate of $3.33 \times 10^{-4}\,s^{-1}$ and using an extensometer to record the strain. Test temperatures at 100 and 150 °C were controlled within $\pm$ 1 °C.

Compression tests were conducted at 25 and 100 °C, as per ASTM standard E-9, on cylindrical specimens (13 mm in diameter by 38 mm in height) using a strain rate of $3.33 \times 10^{-4}\,s^{-1}$ and an extensometer for measuring the strain.

To characterize the wear (and friction) behaviour of the squeeze-cast Zn–32Al and composites in lubricated conditions conforming to contact sliding, block-on-ring wear tests were carried out using a Falex 1 test machine according to the method described by Risdon *et al.* [5]. This provides a rapid, comparative tribological evaluation of materials when sliding, under low bearing stress, against a steel counter-surface [5]. Test conditions were the same as those used by Risdon *et al.* except that the specimens were slid against AISI 4620 steel rings rather than AISI 1144 rings. The 4620 Falex test rings had the same hardness (R_c 22–26) and surface finish (0.56–0.71 μm, r.m.s.) as the 1144 rings. The block contact surfaces were ground to match closely the radius of curvature of the ring outer surface. Testing involved holding the blocks against the rotating steel ring under a load of 690 N (6.9 MPa nominal bearing stress) and sliding for 22 h at a speed of 0.15 $m\,s^{-1}$. The lubricant used was an ISO grade 68 hydraulic oil, heated to 50 °C. A preliminary running-in of the specimens under 0.9 MPa for 15 min preceded the actual tests. Test conditions are similar to those under which Zn–Al alloys are currently used in tribological applications [6].

Fractographic analyses were performed upon selected tensile and compression specimens by scanning electron microscopy.

3. Results

3.1. Metallography

The microstructures of permanent-mould cast and sand-cast Zn–Al alloys have been described in detail [6, 7]. Zn–Al alloys are known to have relatively complex multi-phase microstructures. The binary phase diagram of these alloys is given in Fig. 2. In the case of a Zn–Al alloy containing 32% aluminium (Zn–32Al), solidification of the melt begins with the formation of aluminium-rich dendrites (α phase) and proceeds with the formation of proeutectic β phase around the primary dendrites. The residual liquid solidifies in the interdendritic regions according to the eutectic transformation. Upon subsequent cooling, the β phase regions transform according to the eutectoid reaction into lamellae of α and η phases. A copper-rich ε phase ($CuZn_4$), is formed in the zinc-enriched η phase in copper-containing alloys. Iron is present in the form of faceted $FeAl_3$ particles in Zn–Al alloys.

The microstructure of the squeeze-cast unreinforced Zn–32Al alloy was observed using the back scattered electron (BSE) mode of the scanning electron microscope to provide an atomic contrast image (Fig. 3). In this figure, the dark regions (1) represent the primary cores of aluminium-rich α + η eutectoid which are surrounded by light regions (2) of zinc-rich α + η eutectoid. The light regions display a continuous rim of fine η precipitate in an α matrix (3), resulting from eutectoid transformation of the proeutectic β. The white interdendritic regions are zinc-rich η phase (4) with islands of α + η phase resulting from the transformation of the eutectic β phase. Etching the sample with 2% Nital reagent revealed the presence of ε phase precipitates (5) contiguous to the zinc-enriched η regions (Fig. 4). The composition of each of these phases was confirmed by electron microprobe analyses.

The incorporation of fibres in the Zn–32Al alloy had a significant effect on the size of dendrites in the matrix alloy. As shown in Fig. 5a–c, the size of dendrites is reduced as the volume fraction of fibres is

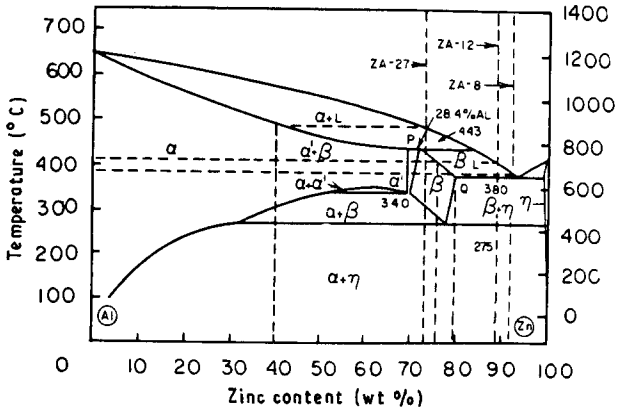

Figure 2 The Zn–Al phase diagram.

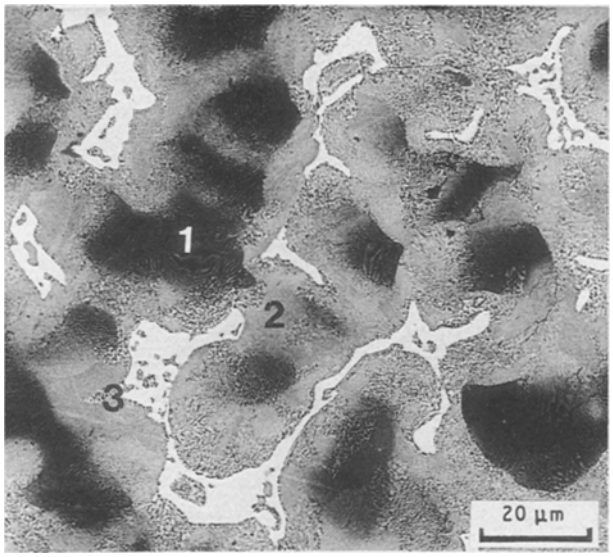

Figure 3 Scanning electron micrograph of as-polished, unreinforced squeeze-cast Zn–32Al showing: (1) primary aluminium-rich eutectoid, (2) zinc-rich eutectoid, (3) η in α matrix resulting from proeutectic β.

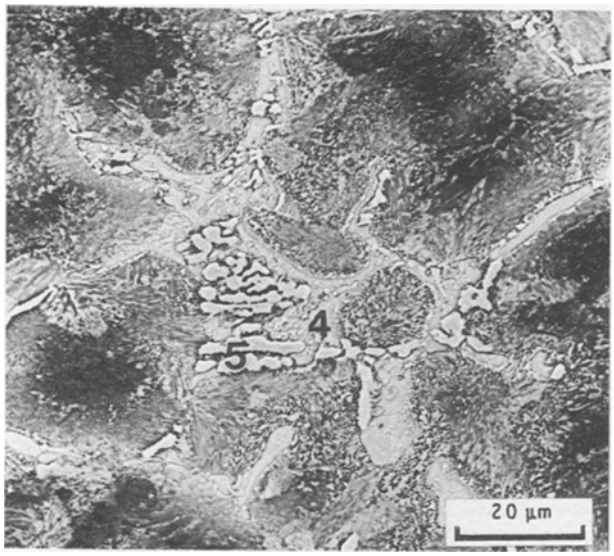

Figure 4 Scanning electron micrograph of Nital etched, unreinforced squeeze-cast Zn–32Al showing (4)η and (5)ε interdendritic phases.

increased. A closer view of the microstructure of fibre-reinforced Zn–32Al shows that the dendrites have grown predominantly into the spaces between fibres, so that the latter are surrounded by zinc-rich phases (Fig. 6a and c). This observation rules out the possibility of fibres acting as nucleation sites for aluminium-rich primary in the matrix alloy. In comparing the reinforced and unreinforced materials, it was found that the volume fraction of η phase decreased with an increase in volume fraction of fibre. When the volume fraction of fibre is 12 vol %, most of the fibres are surrounded by η phase (Fig. 6b). However, when the volume fraction of fibre is 24% (Fig. 6d), the percentage of η phase is much less and most of the fibres are surrounded by zinc-rich α + η eutectoid.

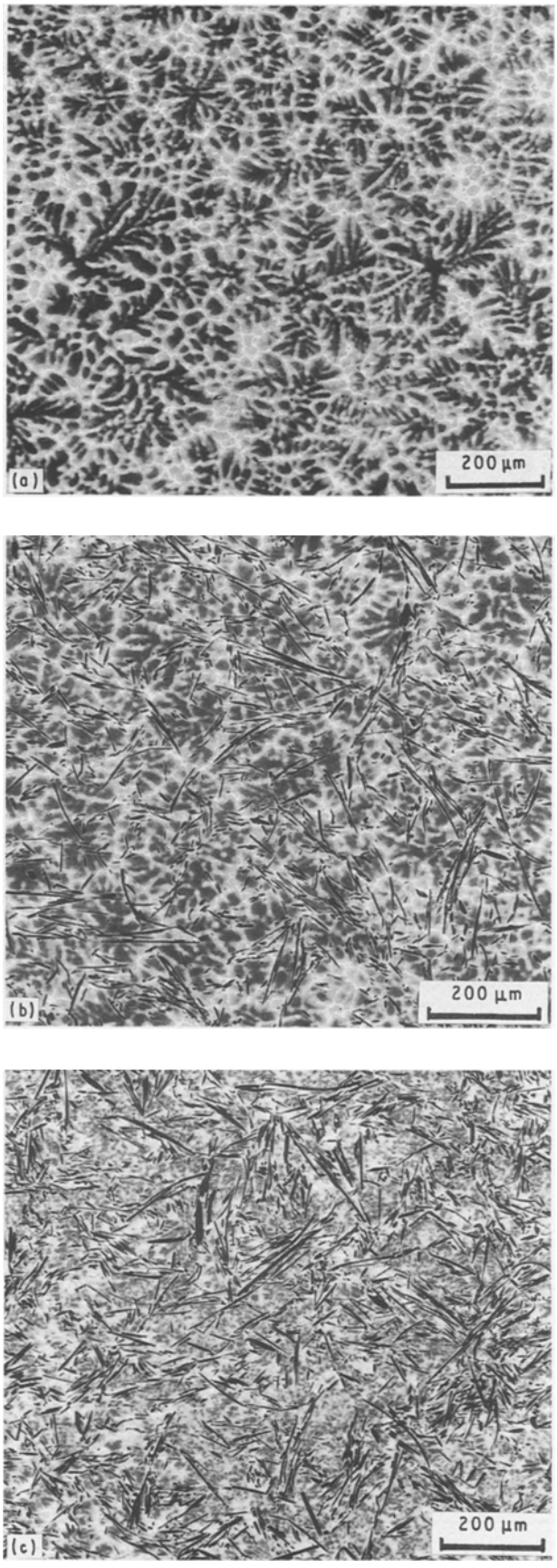

Figure 5 Back scattered electron micrographs of (a) unreinforced Zn–32Al, (b) 12 vol % Al_2O_3 reinforced Zn–32Al, (c) 24 vol % Al_2O_3 reinforced Zn–32Al.

3.2. Tensile properties

Table II lists the tensile test results of the squeeze-cast Zn–32Al alloy and composites. It is clear that at room temperature, the unreinforced alloy exhibits

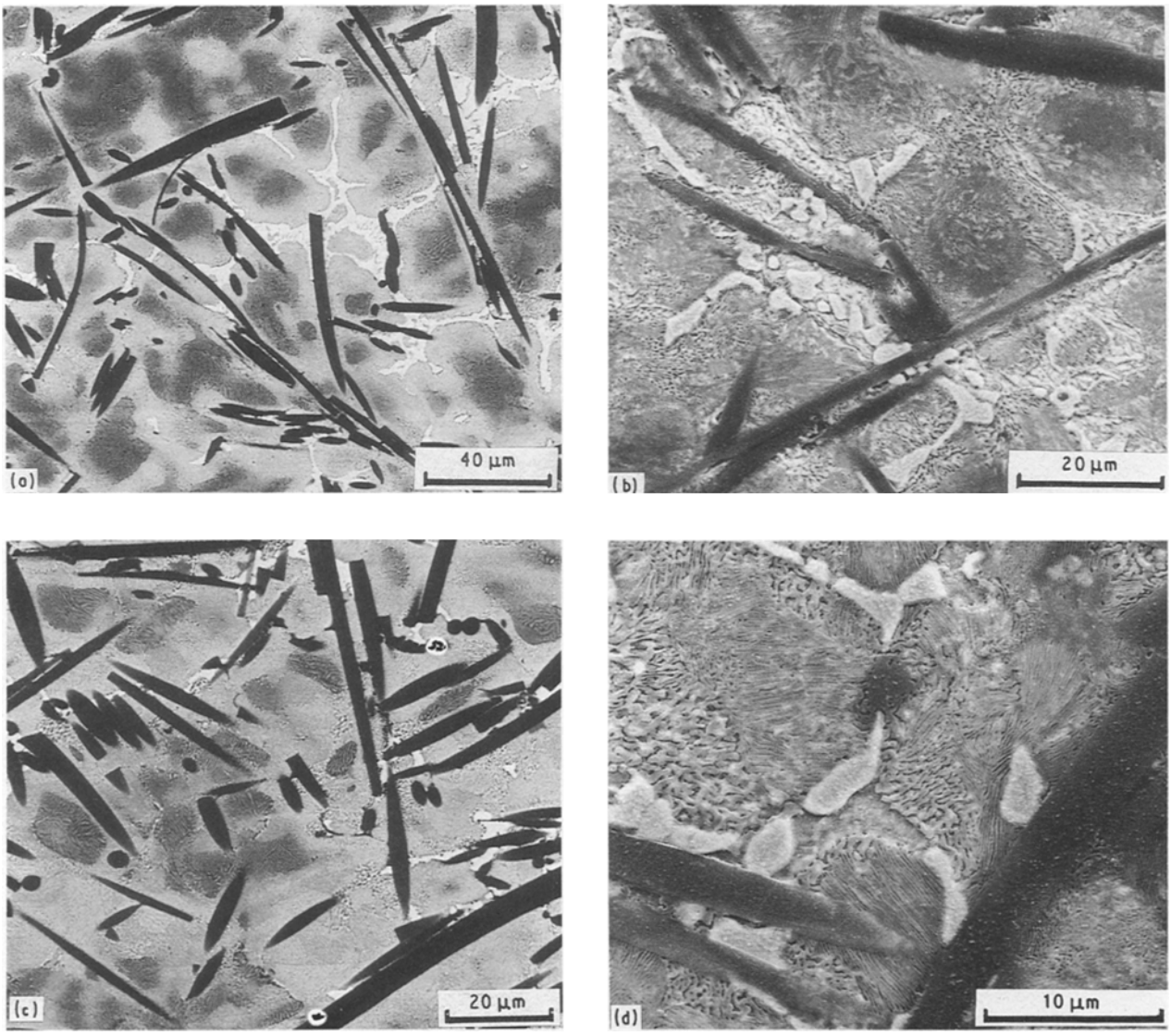

Figure 6 Scanning electron micrographs of (a, b) 12 vol % Al_2O_3 reinforced Zn–32Al, and (c, d) 24 vol % Al_2O_3 reinforced Zn–32Al. (a, c) As-polished, (b, d) Nital etched.

TABLE II Uniaxial tensile test results for squeeze-cast Zn–32Al and fibre-reinforced Zn–32Al composites

Material	Test temperature (°C)	YS (MPa)	UTS (MPa)	Elongation (%)
Unreinforced Zn–32Al	25	333 ± 19	404 ± 13	7–13
	100	199 ± 12	268 ± 7	16–18
	150	101 ± 6	156 ± 3	7–13
12 vol % Al_2O_3 reinforced Zn–32Al	25	–	288 ± 11	0.03–0.25
	100	194 ± 17	219 ± 23	0.60–1.23
	150	124 ± 15	142 ± 19	2.24–2.66
24 vol % Al_2O_3 reinforced Zn–32Al	25	–	293 ± 23	0.05–0.11
	100	251 ± 10	260 ± 17	0.18–0.44
	150	170 ± 14	183 ± 14	0.32–0.52

significantly higher tensile strength than its reinforced counterparts. However, at elevated temperature, the benefits of fibre reinforcement begin to show by providing improved strength, especially in the 24 vol % Al_2O_3 reinforced material. This is most apparent when the UTS of the unreinforced and reinforced materials are compared for the three test temperatures (Fig. 7). The tensile elongation of the fibre-reinforced composites was also reduced in comparison with the unreinforced Zn–32Al alloy (Table II). At room temperature, elongation values of 7%–13% were measured for the unreinforced specimens whereas the composites showed elongations of 0.03%–0.25%. It was not therefore possible to measure a tensile yield strength (0.2% offset) for the composites at room temperature. At elevated temperatures, comparison of

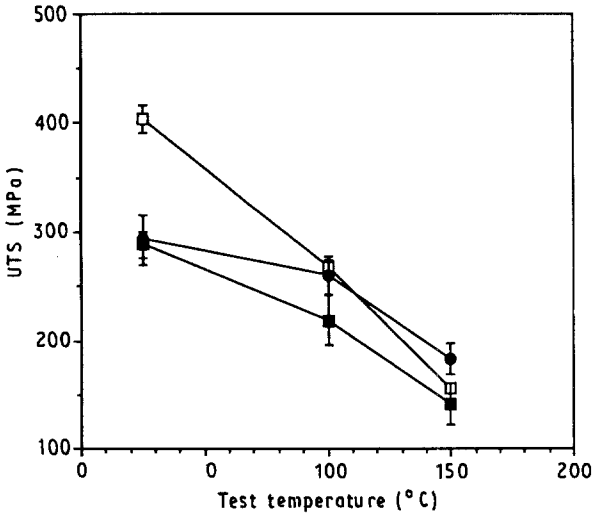

Figure 7 Plot of ultimate tensile strength as a function of test temperature for squeeze-cast Zn–32Al alloy and composites. (□) Zn–32Al, (■) 12% Al_2O_3/Zn–32Al, (●) 24% Al_2O_3/Zn–32Al.

yield strength values for the three materials reveals similar trends as for the UTS.

3.3. Compression properties

The 0.2% offset yield strength of the compression test results is summarized in Table III. The compressive yield strength (CYS) of the squeeze-cast Zn–32Al is significantly higher than the tensile yield strength, especially at room temperature. This is probably related to the presence of tensile residual stresses in the material resulting from the squeeze-casting operation. It is possible that the residual stresses are relieved at 100 °C, resulting in a smaller difference between the tensile and compressive properties at this temperature.

The per cent increase in CYS due to the fibre reinforcement is also shown in Table III. The per cent increase in CYS due to 12 vol % reinforcement is similar at both 25 and 100 °C. However, with 24 vol % reinforcement, this per cent increase is almost double that at room temperature. The compressive yield strength of the composites has proved to be more of a combination of the properties of the metal matrix and of the ceramic reinforcement than the tensile yield strength. It is well known that ceramics are stronger in compression than in tension. CYS increases significantly as the volume fraction of fibres increases and at 100 °C, the CYS of the 24 vol % Al_2O_3/Zn–32Al is about the same as that of the unreinforced Zn–32Al at 25 °C.

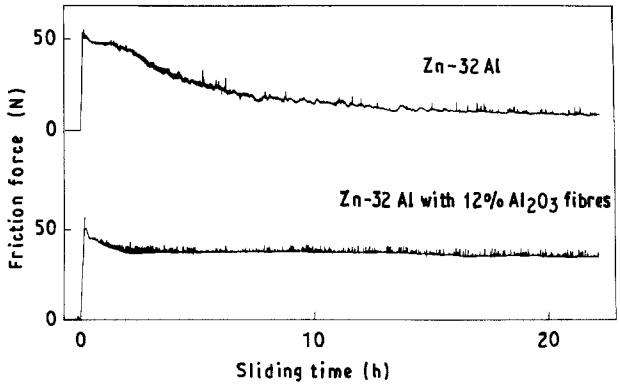

Figure 8 Friction force recordings typical of Zn–32Al and Al_2O_3 reinforced Zn–32Al blocks specimens sliding against steel.

3.4. Wear properties

Fig. 8 illustrates chart recordings of the friction force from block-on-ring tests typical of the squeeze-cast Zn–32Al material or either one of the alumina-fibre-reinforced Zn–32Al composites. These clearly show that the fibre composites always attain steady state sliding conditions much sooner than the unreinforced Zn–32Al material. Table IV summarizes all of the wear and friction results obtained. Following Risdon *et al.* [5], the mean friction coefficient is defined as the average of values read from the chart recording every 2 h. Block height, measured by digital micrometer at the ends and centre of the specimens before and after testing confirmed both the relative magnitude and direction of the weight change data in Table IV and also showed that the dimensional changes for the composite specimens occurred mainly at the centre position. It is recorded here that similar friction and wear data was obtained in earlier replicate tests with block samples which inadvertently had been ground to a slightly smaller radius than the rings. Thus, the present results are reported as representative of the three types of material with more confidence than the data in Table IV might otherwise suggest.

The typical appearance of specimen pairs after lubricated sliding tests of unreinforced and reinforced Zn–32Al blocks are shown in Fig. 9. Wear takes place over the entire bearing surface of the Zn–32Al blocks, whereas rubbing marks on blocks of either the 12% or 24% alumina fibre composites were mainly on the central portion of the surface. This limited contact between specimens results from the slight (but necessary) non-conformity of the ring and block specimen radii of curvature but, more importantly, it confirms

TABLE III Compressive yield strength for unreinforced and fibre reinforced Zn–32Al

Material	CYS (MPa) at 25 °C (% increase in CYS compared to Zn–32Al)	CYS (MPa) at 100 °C (% increase in CYS compared to Zn–32Al)
Zn–32Al	378 ± 5	211 ± 25
12 vol % Al_2O_3/Zn–32Al	463 ± 3 (22.5%)	253 ± 12 (20%)
24 vol % Al_2O_3/Zn–32Al	511 ± 15 (35%)	355 ± 3 (68%)

TABLE IV Wear and friction results for squeeze-cast unreinforced and Al_2O_3-fibre-reinforced Zn–32Al specimens in lubricated sliding against AISI 4620 steel

Specimen blocks	Block weight loss (mg)	Block wear rate ($mg\,h^{-1}$)	Ring weight loss (mg)	Ring wear rate ($mg\,h^{-1}$)	Mean coefficient of friction
Zn–32Al	15.7	0.71	1.0	0.046	0.035
	14.4	0.65	3.1	0.142	0.035
12 vol % Al_2O_3	(− 2.4)[a]	–	(− 0.1)	–	0.057
Zn–32Al	(− 3.0)	–	0.43	0.020	0.058
24 vol % Al_2O_3	(− 3.6)	–	0.1	0.005	0.057
Zn–32Al	(− 3.2)	–	0.5	0.023	0.044
	(− 2.2)	–	0.42	0.019	0.039

[a] Figures in parentheses indicate weight gain.

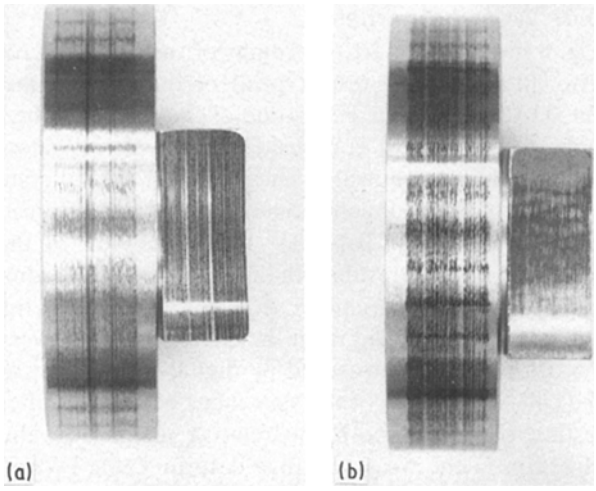

Figure 9 Specimen bearing surfaces after sliding of (a) Zn–32Al and (b) 24 vol % Al_2O_3 reinforced Zn–32Al blocks against AISI 4620 steel rings.

that little wear has taken place on the composite block specimens. SEM and energy-dispersive X-ray analysis (EDX), Fig. 10, provides additional evidence that sliding contact occurred only in the middle of the composite block specimen's bearing surface.

3.5. Fractography

Metallographic examinations were performed on Zn–32Al tensile specimens sectioned in a plane perpendicular to the fracture surface and polished. It was noted that for specimens tested at 25 °C, the fracture mode was primarily transgranular, although occasionally cracks propagated through the η phase and along the η/zinc-rich eutectoid interfaces. When the material was tested at 150 °C, the fracture path was found to proceed preferentially along the η/zinc-rich eutectoid interfaces and through the η phase, resulting in a fully interdendritic failure (Fig. 11). It is believed that at the higher test temperatures, the transition from a transgranular to an intergranular mode of failure resulted in decreased strength and lowered ductility of the unreinforced material. This transition is likely due to the weakening of the η phase and η/zinc-rich eutectoid interfaces at elevated temperatures. These findings correlate well with the tensile strength and elongation values listed in Table II.

In the case of the composite materials, the fracture behaviour of specimens reinforced with 12 and 24 vol % Al_2O_3 fibres was found to be quite similar (Fig. 12a and b). Cracking proceeded preferentially along the fibre/matrix interfaces, and occasionally along the η/zinc-rich eutectoid interfaces (Fig. 13). This suggests that the fibre/matrix interfacial strength is weaker than the η/zinc-rich eutectoid interfacial strength. In addition to fibre/matrix debonding, the fracture of fibres as well as fibre pull out were also observed on the fracture surfaces of the composites (Fig. 12a and b). Fine dimples were found in the matrix between the decohered and fractured fibres but no large-scale ductility was observed, even at elevated test temperatures. The fracture surfaces of reinforced specimens tested at elevated temperatures were similar to those of specimens tested at room temperature. The reduced volume fraction of interdendritic η phase, especially in the 24 vol % Al_2O_3 reinforced materials, resulted in the absence of a transition from a transgranular to an intergranular mode of failure which was observed in the unreinforced material. The same fracture mechanisms were observed at 150 °C as at 25 °C, resulting in improved strength at elevated temperature. Considering the degradation in strength of the η phase at elevated temperature, it is conceivable that the fibre/matrix interfacial strength, although weak at 25 °C, nevertheless becomes higher than the η/zinc-rich eutectoid strength at 150 °C.

It has been mentioned above that the SiO_2 binder, which was present on the fibre surfaces of the preform, was retained even after the squeeze-casting operation. Considering that the Al_2O_3 fibres are almost completely covered by this SiO_2 film, the fibre/matrix interfaces actually consist of Al_2O_3/SiO_2/Zn–32Al layers. It is possible that fracture could propagate either along the SiO_2/Zn–32Al or the Al_2O_3/SiO_2 interfaces, or through the SiO_2 layer. Auger electron spectroscopy (AES) of *in situ* fracture surfaces of 24 vol % Al_2O_3 reinforced Zn–32Al showed that fracture occurs through the SiO_2 binder layer present at the fibre/matrix interface. AES point analyses and compositional depth profiles demonstrated that SiO_2 was present both on the fibre surfaces and in the depressions left in the matrix by decohered fibres [8].

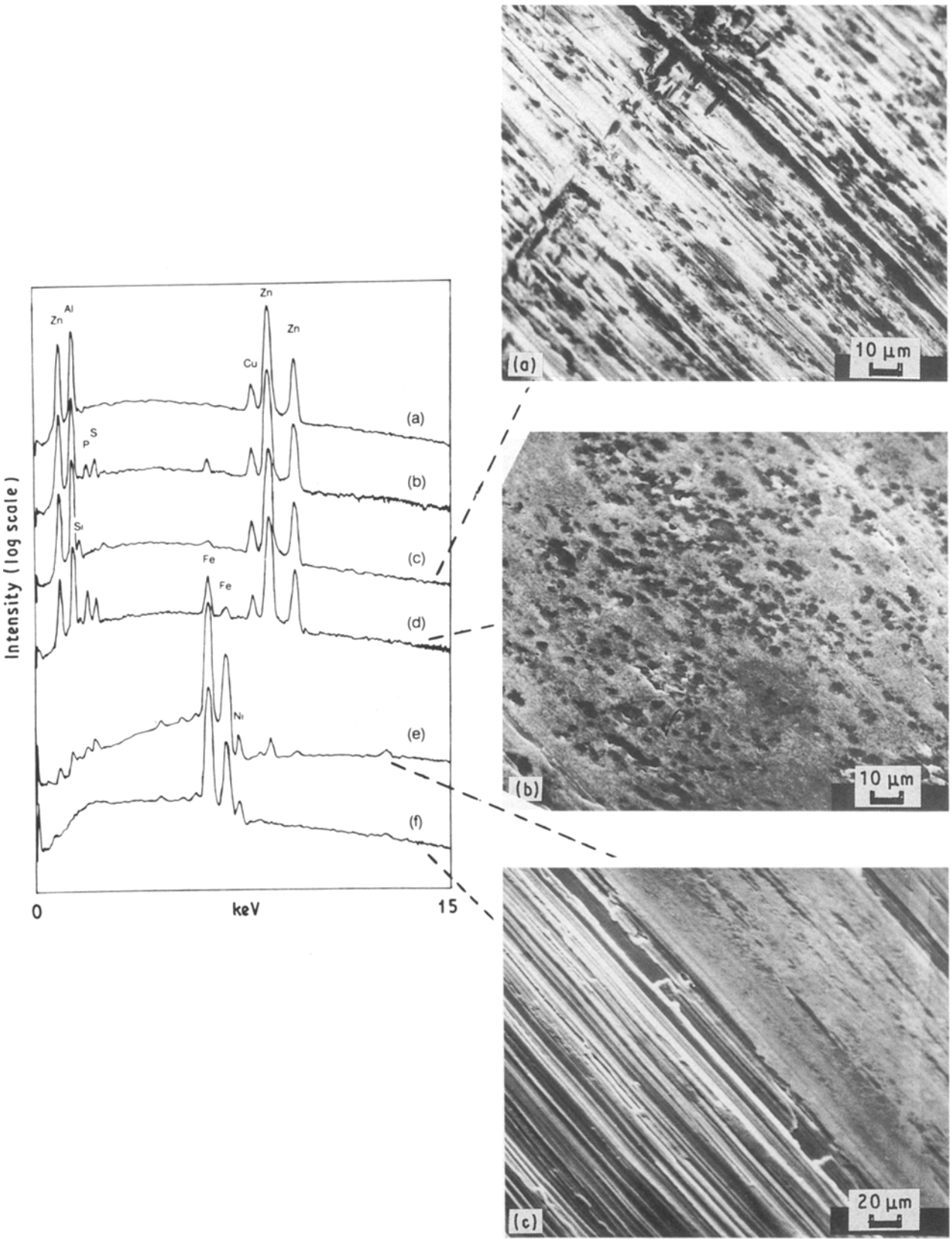

Figure 10 EDX spectra of virgin and tested specimen surfaces. (a) Virgin Zn–32Al block, (b) worn Zn–32Al block, (c) outer area of 24 vol % Al_2O_3/Zn–32Al block after testing, (d) central area of same specimen surface as in (c), (e) worn area of AISI 4620 steel ring after testing, (f) virgin area of same steel ring.

Some of the fibre-reinforced compression specimens were loaded to failure (about 5% strain) and the resulting fracture surfaces were examined in the SEM. The fracture surfaces of the specimens were composed of shear failure of the Zn–32Al matrix with some cracked fibres (Fig. 14). Specimens were sectioned and polished in a plane perpendicular to the fracture surface. It was observed that the extent of fibre/matrix decohesion appeared to be much reduced although there was significant fibre cracking in the region directly underneath the fracture surface. The shear stresses generated by the compressive loading caused

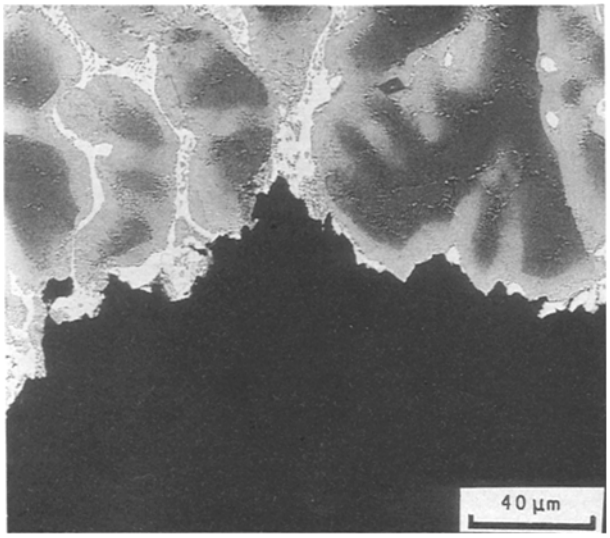

Figure 11 Fracture profile (BSE micrograph) of a squeeze-cast, unreinforced Zn–32Al tensile specimen tested at 150 °C showing preferential fracture of interdendritic regions.

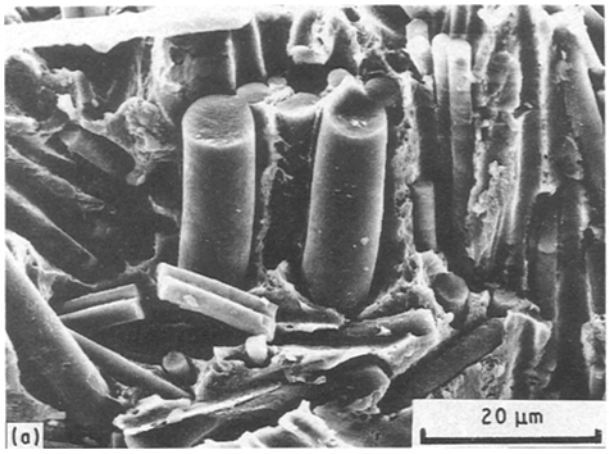

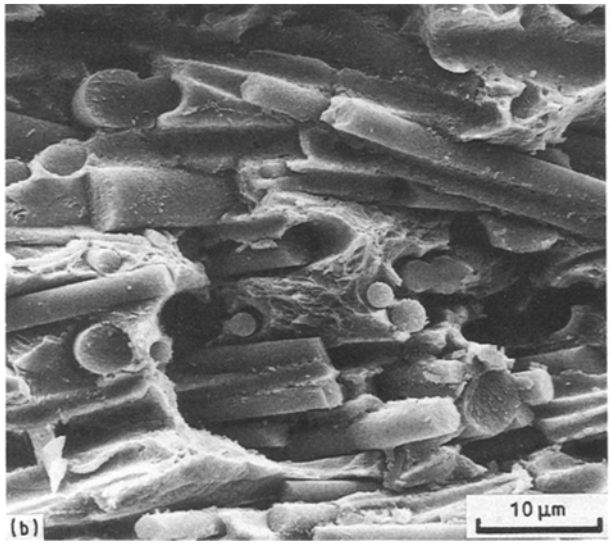

Figure 12 Scanning electron fractographs of tensile specimens tested at 25 °C: (a) 12 vol % Al_2O_3 reinforced Zn–32Al; (b) 24 vol % Al_2O_3 reinforced Zn–32Al.

bending and realignment of the fibres perpendicular to the plane of maximum shear stress. This realignment was accompanied by extensive cracking of the rigid fibres. As a result of this phenomenon, the fibres

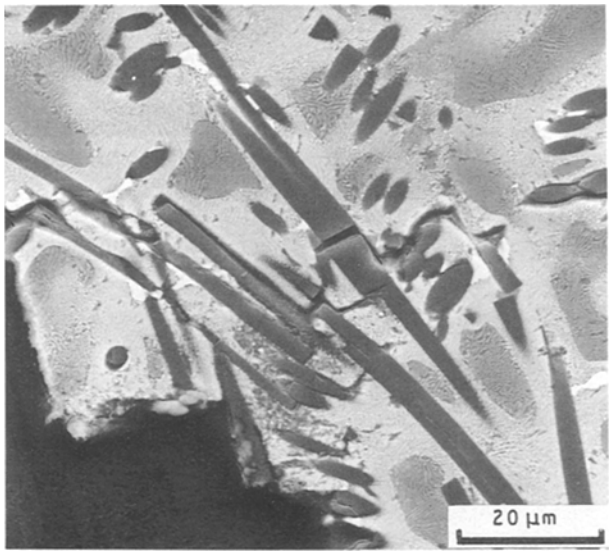

Figure 13 Atomic contrast image (BSE micrograph) of a sectioned and polished tensile specimen of 24 vol % Al_2O_3 reinforced Zn–32Al (test temperature 25 °C) showing fibre/matrix debonding and cracking of fibres.

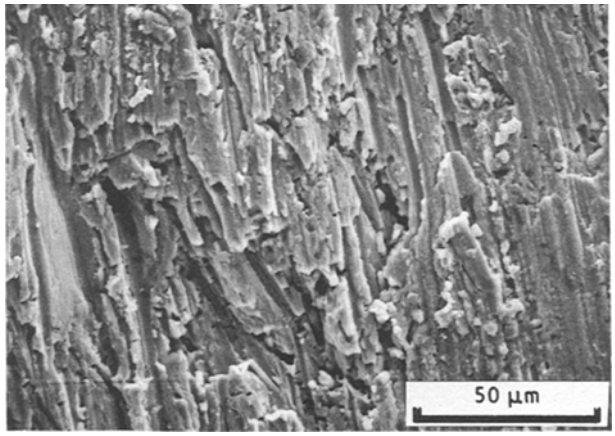

Figure 14 Scanning electron fractograph of a 24 vol % Al_2O_3 reinforced Zn–32Al specimen failed in compression at 25 °C.

appearing on the fracture surface were mostly fractured through their thickness. It is obvious from these observations that the compressive mode of loading decreases the tendency of the reinforced materials to fail prematurely at the brittle fibre/matrix interfaces, resulting in higher properties in compression than in tension.

4. Discussion

The present study shows that the incorporation of alumina fibres in the Zn–32Al alloy affects the microstructure of the unreinforced alloy. It was found that as the volume fraction of fibre reinforcement increased, both the dendrite size and volume fraction of interdendritic phases decreased. In a preform, the Al_2O_3 fibres are held together in a three-dimensional interconnecting network by an SiO_2 binder. During the squeeze-casting operation, the molten Zn–32Al

alloy infiltrates this network and then solidifies between the fibres. When the fibre volume fraction is increased, the fibre spacing decreases, resulting in finer dendrite sizes in the squeeze-cast product. Considering that the thermal conductivity of the ceramic fibres is smaller than that of the Zn–Al alloy and because the preform is preheated prior to squeeze-casting, the overall cooling rate is probably lower for the reinforced castings than for the unreinforced alloy. As a result, the extent of dendritic segregation in the reinforced alloys is lower and a more homogeneous microstructure is obtained.

The incorporation of alumina fibres in Zn–32Al also affects the mechanical properties of Zn–32Al alloy. From the limited test data, it was shown that fibre reinforcement improved the tensile and compression properties of Zn–32Al at elevated temperatures, but the improvements were accompanied by a substantial decrease in ductility. The ultimate tensile strength of the unreinforced squeeze-cast Zn–32Al dropped from 404 MPa at 25 °C to 156 MPa at 150 °C, whereas the UTS of the 24 vol % Al_2O_3 reinforced Zn–32Al decreased from 293 MPa at 25 °C to 183 MPa at 150 °C. The low room-temperature strength and ductility of the composites is believed to be caused by the presence of the brittle SiO_2 binder at the fibre/matrix interfaces. This is confirmed by the observation that the dominant failure mode in the composite materials was fibre/matrix decohesion. In the case of the unreinforced Zn–32Al, the failure mode was transgranular at 25 °C and intergranular at 150 °C. This transition in the fracture mode is probably due to the weakening of the interdendritic η and η/zinc-rich eutectoid interfaces at elevated temperatures. However, there was no change in the failure mode of the composites as the test temperature was raised from 25 °C to 150 °C. This might be due to the insensitivity of the fibre/matrix interfacial strength to temperature. The 24 vol % Al_2O_3/Zn–32Al composite has a higher UTS than the 12 vol % Al_2O_3/Zn–32Al at 150 °C (183 MPa versus 142 MPa) because of the smaller volume fraction of interdendritic phases in the composite with the higher fibre content. These results indicate that the fibre/matrix interfacial strength, albeit low at 25 °C, becomes higher than that of the interdendritic η phase and η/zinc-rich eutectoid interfaces at elevated temperature [9].

When the squeeze-cast materials were loaded in compression, it was found that the compressive yield strength of the 12 and 24 vol % Al_2O_3 reinforced materials was higher than that of the unreinforced alloy both at room and elevated temperatures. Specimens loaded to failure revealed that under compressive loading, the composite materials tended to fracture by ductile failure of the Zn–32Al matrix along a plane of maximum shear stress. Little fibre/matrix debonding was observed because the stresses acting upon the fibre/matrix interfaces under this mode of loading were not oriented in such a manner as to promote failure of the brittle interfacial layer.

The data in Table IV show that addition of 12 or 24 vol % Al_2O_3 fibres into the Zn–32Al matrix renders the specimen block wear undeterminable by the weight loss method because slight weight gains are measured. Along with the dimension change, visual and microscopic evidence, this indicates that specimen wear during lubricated sliding in the present tests was much reduced by the fibre reinforcement. Counter-surface (ring) wear was also reduced, but mean friction values are somewhat greater for the composites.

In Table V, the present results are compared with data similarly obtained by Risdon *et al.* [5] on ZA-27 alloys prepared by various methods. The mean wear rate and friction coefficient of the squeeze-cast Zn–32Al alloy are greater than corresponding values for sand-cast ZA-27, and less than those of pressure die cast or permanent moulded ZA-27 material, in lubricated sliding against steels of similar hardness and initial surface roughness.

The EDX spectra of the solvent-cleaned, worn surfaces shows the presence of both elements from the mating specimens (iron on the blocks, zinc and aluminium on the rings), and those (phosphorus and sulphur) from the anti-wear additive (zinc dialkyldithiophosphate) in the lubricant. Discrete particles of the mating surface material were not observed on worn surfaces, and X-ray mapping showed that all foreign elements were evenly distributed over the wear marked areas. Together with smeared appearance of these areas, for example in Fig. 11, this suggests that a very thin "third-body" layer of compacted, extremely fine wear debris forms at the sliding interface, in common with many other tribosystems [13]. A boundary film, containing phosphorus and sulphur, formed by

TABLE V Comparison of present wear and friction measurements for Zn–32Al and composites with data of Risdon *et al.* [6] for ZA-27 in lubricated sliding against AISI 1144 steel

Material	Wear rate ($mg\,h^{-1}$)	Friction coefficient
Sand cast ZA-27 (< 0.2 vol % porosity)[a]	0.13	0.01
Sand cast ZA-27 (0.5–1.0 vol % porosity)[a]	0.24–0.36	0.01
Pressure die cast ZA-27[a]	1.02	0.08
Permanent moulded ZA-27[a]	1.4–4.5	0.03–0.07
Squeeze-cast Zn–32Al	0.65–0.71	0.035
12 vol % Al_2O_3/Zn–32Al	nil[b]	0.057–0.058
24 vol % Al_2O_3/Zn–32Al	nil[b]	0.039–0.057

[a] Composition of ZA-27 (wt %): 25.0–28.0 Al, 2.0–2.5 Cu, 0.01–0.02 Mg [9].
[b] Weight gain of the blocks was measured.

reaction of the anti-wear additive with the metal surfaces may also be present, separately from or as part of this interfacial layer.

Although the crudely averaged friction and wear data allow comparisons with reported work [6], further examination of the present results provides additional information on the comparative behaviour of the unreinforced and fibre-reinforced Zn–32Al materials. Thus, as shown in Fig. 9, the Zn–32Al specimens exhibit a slowly decreasing friction coefficient, from about 0.08 to an equilibrium value of 0.02. This probably reflects extended running-in processes of both increasing contact conformity due to wear of the block, and gradual formation of low-friction debris and boundary lubrication films. On the other hand, the shorter time for friction to decrease to a steady value with the composite blocks may be the consequence of a more limited wearing-in period. The higher steady-state friction coefficient, of about 0.05, could result from different rheological properties of the wear debris film, which now will contain material from the Al_2O_3 fibres. This film may also give better protection to both of the first body surfaces, through enhanced load-bearing capabilities [13], thus contributing to their reduced wear in this tribosystem. Alternatively, preferential load-bearing by the higher modulus fibre reinforcement in the composites could give rise to greater penetration of asperities into either wear debris or boundary lubricant films and, thus, result in higher frictional interactions. However, this would tend to promote greater wear and so is a less likely explanation of the present results.

In view of the above findings, it is expected that if the fibre/matrix interfacial strength could be increased, improved room-temperature tensile strength, ductility and toughness could be achieved in the Al_2O_3/Zn–32Al composites. This study has demonstrated that even under conditions of poor fibre/matrix bonding, Al_2O_3 fibre reinforcement does result in improved compression, wear and elevated temperature tensile properties. Fibre/matrix interfacial strength in these composites can be improved by optimizing the amount of SiO_2 binder used to hold the fibre together, thereby reducing the size and number of brittle SiO_2 patches at fibre contact points. Another alternative would be to use a different kind of binder, having better mechanical properties than SiO_2.

5. Conclusions

1. Alumina fibres in squeeze-cast discs of Al_2O_3 reinforced Zn–32Al were found to be aligned randomly in the transverse plane, retaining the fibre arrangement of the preform. The squeeze-cast materials were metallurgically sound, with no porosity and good fibre/matrix wetting.

2. Microstructures of Zn–32Al and Al_2O_3/Zn–32Al squeeze-cast materials were composed of aluminium-rich primary dendrites of $\alpha + \eta$ eutectoid, of zinc-rich $\alpha + \eta$ eutectoid and of interdendritic phases composed of η and ε ($CuZn_4$). The dendrite size and volume fraction of interdendritic phases were found to decrease as the volume fraction of Al_2O_3 fibres was increased.

3. Although the unreinforced Zn–32Al had higher tensile strength than its reinforced counterparts at room temperature, reinforcement with alumina fibres did provide improved elevated temperature (100 and 150 °C) tensile properties.

4. Compressive yield strength (CYS) of the squeeze-cast Zn–32Al increased significantly as the volume fraction of fibres was increased. At 100 °C, the CYS of the 24 vol % Al_2O_3/Zn–32Al was 68% higher than that of the unreinforced Zn–32Al at 100 °C.

5. Block-on-ring wear test results indicated an improved wear resistance of Al_2O_3 fibre-reinforced Zn–32Al in lubricated sliding against steel compared with the squeeze-cast, unreinforced Zn–32Al and with ZA-27 alloys formed by various processes.

6. The reduced wear of both composite specimen block and steel ring countersurface, and the slightly higher equilibrium friction of this tribosystem, compared with that of the unreinforced Zn–32Al material, are explicable on the basis of different properties of the respective "third-body" films generated at the sliding interface.

7. It is considered that the poor ductility of the Zn–32Al composites is related to the presence of a brittle SiO_2 layer at the fibre/matrix interfaces. This SiO_2 layer, which is the binder holding the fibres together in the preform, resulted in extensive fibre/matrix decohesion under tensile loading, severely impairing the performance of the reinforced materials.

Acknowledgements

The authors thank Noranda Technology Centre for the supply of Zn–Al based composites, Dr M. Shehata and Mr B. Casault, MTL, CANMET, for performing the quantitative metallographic examination, Mr R. Bouchard, G. Weatherall and P. Fryzuk for performing the mechanical tests (tensile, compression, impact and fatigue), and Mrs V. Moore for doing the microprobe analyses.

References

1. B. MAGNUS, M. MELUS and G. CROEG, *La Fonderie Belge* **4** (1982) 1927.
2. A. A. DAS, B. ZANTOUT, M. M. YAKOUB and A. J. CLEGG, in "International Symposium on Zinc–Aluminium (ZA) Casting Alloys", edited by G. P. Lewis, R. J. Barnhurst and C. A. Loong, Series 25-5/1, No. 1 (Canadian Institute of Mining and Metallurgy, Montréal, Québec, 1986) p. 213.
3. R. GUERRIERO, J. B. PARSE and I. TANGERINI, *ibid.* p. 229.
4. P. N. DENT and S. MURPHY, *ibid.*, p. 127.
5. T. J. RISDON, R. J. BARNHURST and W. M. MIHAICHUK, in "Comparative Wear Rate Evaluation of Zinc–Aluminum (ZA) and Bronze Alloys through Block on Ring Testing and Field Applications", SAE Paper No. 860064 (1986) p. 1.
6. R. J. BARNHURST, E. GERVAIS and F. D. BAYLES, *AFS Trans.* **91** (1983) 569.
7. M. SAHOO, L. V. WHITING, V. CHARTRAND and G. WEATHERALL, *ibid.* **94** (1986) 225.
8. L. DIGNARD-BAILEY, S. DIONNE and S. H. LO, in

"Proceedings of Symposium on Fundamental Relationships between Microstructure and Mechanical Properties of Metal-Matrix Composites" (The Minerals, Metals and Materials Society, Warrendale, PA, 1990) p. 23.
9. S. H. LO, S. DIONNE, L. DIGNARD-BAILEY, M. SAHOO and J. C. FARGE, in "International Symposium on Processing of Ceramics and Metal Matrix Composites", edited by H. Mostaghaci, The Metallurgical Society of CIM, Proceedings Vol. 17 (1989) p. 412.
10. M. GODET, *Wear* **136** (1990) 29.

Received 17 June
and accepted 16 December 1991